

## Investigation of cavity modes and direct observation of Purcell enhancement in 2D photonic crystal defect microcavities

A. Kress, F. Hofbauer, N. Reinelt, Hubert J. Krenner, Max Bichler, Dieter Schuh, R. Meyer, Gerhard Abstreiter, Jonathan J. Finley

### Angaben zur Veröffentlichung / Publication details:

Kress, A., F. Hofbauer, N. Reinelt, Hubert J. Krenner, Max Bichler, Dieter Schuh, R. Meyer, Gerhard Abstreiter, and Jonathan J. Finley. 2005. "Investigation of cavity modes and direct observation of Purcell enhancement in 2D photonic crystal defect microcavities." *Physica E: Low-dimensional Systems and Nanostructures* 26 (1-4): 351–55.  
<https://doi.org/10.1016/j.physe.2004.08.075>.

# Investigation of cavity modes and direct observation of Purcell enhancement in 2D photonic crystal defect microcavities

A. Kress\*, F. Hofbauer, N. Reinelt, H.J. Krenner, M. Bichler, D. Schuh,  
R. Meyer, G. Abstreiter, J.J. Finley

*Walter Schottky Institut, Am Coulombwall 3, Technische Universität München, 85748 Garching, Germany*

## Abstract

We demonstrate our ability to control and manipulate the optical modes in 2D Photonic Crystal Defect cavities and investigate their coupling to InGaAs self-assembled quantum dots. Our results enable us to probe the nature of individual cavity modes and directly investigate cavity QED phenomena. For the lowest mode volume cavities investigated, consisting of a single missing air hole within a hexagonal lattice, we have measured a clear Purcell enhancement of the light-matter interaction in the weak coupling regime. For QDs on-resonance with localized cavity modes this translates to a shortening of the quantum dot spontaneous emission lifetime by a factor  $\sim 2$  when compared to off-resonance dots.

There is currently much interest in using individual quantum dots (QDs) as deterministic single photon sources for quantum cryptography applications [1]. Individual QDs are naturally capable of generating single photons since their inter-band optical response depends strongly on carrier occupation and, providing that the QD repopulation rate exceeds the spontaneous emis-

sion lifetime, regulated single photon emission is guaranteed at a specific frequency. Single photon generation using QDs has now been demonstrated by a number of groups worldwide [2–4] but, for practical applications, the low external quantum efficiency seriously limits their realistic potential [1]. This bottleneck may be overcome by embedding QDs within optical microcavities and utilizing cavity QED phenomena, such as the Purcell effect [5], to promote single photon emission into a specific optical mode. The control of the spontaneous emission from individual dots in the weak

---

\*Corresponding author. Tel.: +49-89-28912784; fax: +49-89-3206620.

E-mail address: kress@wsi.tum.de (A. Kress).

coupling promises the realization of efficient, QD-based single photon emitters with potential for operation at high bit rates in excess of 1 GHz. The strength of the Purcell enhancement in the weak coupling regime is enhanced for optical cavities that combine high-quality factors ( $Q$ ) and small mode volumes ( $V$ ). Recently, a number of groups have started to study 2D-photonic crystal defect (PCD) resonators that combine low  $V \sim (\lambda/n)^3$  and high  $Q$  with a planar geometry, a significant advantage for active photonic devices [6,7]. In this paper, we demonstrate our ability to control and manipulate the optical modes in such PCD cavities and investigate their coupling to InGaAs self-assembled QDs. Our results enable us to probe the nature of individual cavity modes and directly investigate cavity QED phenomena. For the lowest mode volume cavities investigated, consisting of a single missing hole within a hexagonal lattice of air holes we have measured a clear Purcell enhancement of the light-matter interaction in the weak coupling regime. For QDs on-resonance with localized cavity modes this translates to a shortening of the spontaneous emission lifetime by a factor  $\sim 2$  when compared to off-resonance dots.

The samples investigated are grown by MBE and consist of an active AlGaAs–GaAs–Air slab waveguide into which a layer of  $\text{In}_{0.50}\text{Ga}_{0.50}\text{As}$  self-assembled quantum dots are incorporated. The QD density for all samples presented here is  $\sim 300 \text{ QDs}/\mu\text{m}^2$ . The samples were grown on  $n^+$  ( $3 \times 10^{18} \text{ cm}^{-3}$ ) GaAs substrates and nominally consisted of the following layers:  $1 \mu\text{m}$   $n^+$  doped  $\text{Al}_{0.35}\text{Ga}_{0.65}\text{As}$  lower cladding for the waveguide, a  $400 \text{ nm}$  thick GaAs waveguide core into which a layer of InGaAs QDs were embedded. The QD layer was positioned  $100 \text{ nm}$  from the GaAs–AlGaAs interface, at an anti-node of the calculated lowest energy ( $\text{TE}_{00}$ ) guided optical mode. PCD cavities were formed by introducing missing-hole point defects into a deeply etched 2D hexagonal lattice of air holes (see insets–Fig. 1). The crystals are fabricated by firstly depositing a  $120 \text{ nm}$  thick  $\text{Si}_3\text{N}_4$  etch mask before e-beam lithographic patterning. Different PCD cavity patterns were then written into the resist and transferred into the  $\text{Si}_3\text{N}_4$  mask by a reactive ion etching using  $\text{CF}_4$ . Highly anisotropic etching of vertical air holes into

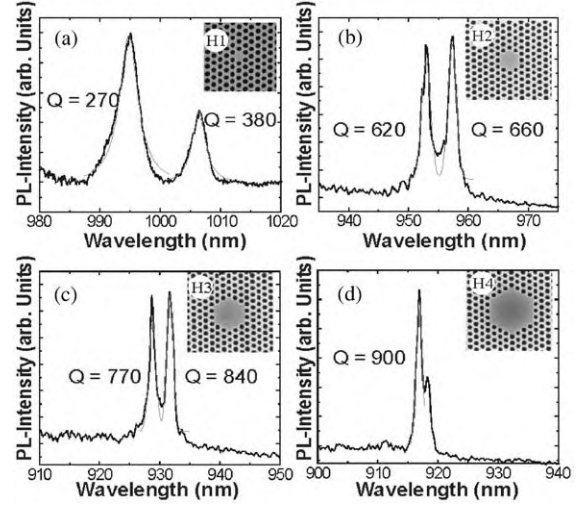


Fig. 1.  $\mu\text{PL}$  spectra and  $Q$ -factors recorded from four typical PCD cavities (a) H1, (b) H2, (c) H3, and (d) H4. The insets show SEM images of the cavities investigated.

the AlGaAs–GaAs waveguide is achieved via a Cl–Ar RIE process. For air holes with a typical diameter of  $\sim 200 \text{ nm}$ , we obtain a depth  $> 1 \mu\text{m}$  and almost perfect perpendicular sidewalls [8].

Optical measurements were performed at  $T = 10 \text{ K}$  using a confocal micro-photoluminescence ( $\mu\text{PL}$ ) system, which enables a spatial resolution of  $\sim 1 \mu\text{m}$ . For CW measurements, excitation was via a HeNe laser at  $\lambda = 632 \text{ nm}$  and the resulting  $\mu\text{PL}$  was dispersed by a  $0.55 \text{ m}$  TRIAX single monochromator and detected using a  $\text{LN}_2$  cooled CCD camera. Time-resolved measurements were performed using pulsed optical excitation at  $\lambda = 650 \text{ nm}$  and a single photon avalanche photodiode (EG&G–SPCM–AQR-200). The excitation pulse FWHM is  $\sim 50 \text{ ps}$  whereas the resolution is limited by the detector to  $\sim 350 \text{ ps}$ . Using deconvolution techniques this approach provides a best time resolution of  $\sim 150 \text{ ps}$ , much shorter than the ground state radiative lifetime of our QDs ( $\sim 1000 \text{ ps}$ ).

Fig. 1 summarizes typical results from our CW  $\mu\text{PL}$  investigations, showing spectra recorded using non-resonant excitation ( $P_{\text{ext}} = 4 \times 10^2 \text{ W}/\text{cm}^2$ ) from a series of PCD cavities with sizes ranging from H1 (single missing hole) to H4 (4 missing holes along the edge of hexagonal defect).

The peak-like structures correspond to localized optical modes within the cavities and contrast strongly with the inhomogeneously broadened ( $\sim 100$  meV FWHM) QD emission detected away from the PCD cavities. The mode  $Q$ -factors ( $Q = \omega/\Delta\omega$ ) range from  $\sim 300$  for a H1 defect up to  $\sim 1000$  for a H4 defect. The periodicity of the photonic crystal is  $a = 300$  nm, leading to a complete in-plane TE photonic bandgap ( $H$ -field along growth direction) between  $\lambda \sim 0.8 \mu\text{m}$  and  $\lambda \sim 1.2 \mu\text{m}$  for an air fill factor of  $A = 55\%$ . The  $Q$ -factors measured in Fig. 1 compare very well with other reports for PCD-cavities fabricated in slab waveguides, demonstrating the high quality of the structures investigated here [9,11]. The slab waveguide design leads here to a predominant loss of cavity photons into the substrate due to the low refractive index step of  $\sim 5\%$  from GaAs to AlGaAs at  $\lambda = 1 \mu\text{m}$ .

We now consider the influence of changing the air hole radius to the periodicity ( $r/a$ ) in the range from 0.30 to 0.42 on the cavity modes. These range of values corresponds to air fill-factors in the range  $A = 0.33\text{--}0.64$ , where  $A = (2\pi/\sqrt{3})(r/a)^2$ . Fig. 2a shows a plot of the wavelength of the cavity modes as a function of ( $r/a$ ) for H1 to H4 PCD cavities. Here we always considered common optical modes of the different cavity sizes, each point being represented by the lower wavelength peak of each emission doublet. These measurements demonstrate our ability to control the wavelength of the cavity modes over a large range ( $\lambda \sim 910\text{--}1030$  nm) with a precision of  $\Delta\lambda \sim 2$  nm. These investigations demonstrate precise control of the cavity modes, over a wider range than presented in recent publications [12]. The control of the wavelength of photonic modes is essential for obtaining coupling of single QDs to photonic states in  $\mu$ -cavities. From Fig. 2a, we observe a linear dependence of the spectral position on the ratio  $r/a$  for each cavity size. This is visualized by the linear fits shown as black lines. Moreover, the shift rate for each mode increases strongly with reducing cavity size. On a basic level, this linear dependence can be considered to reflect the simple modification of the effective cavity length as the radius of the air holes ( $r$ ) increases with a fixed crystal periodicity. For example, for the H1 cavity

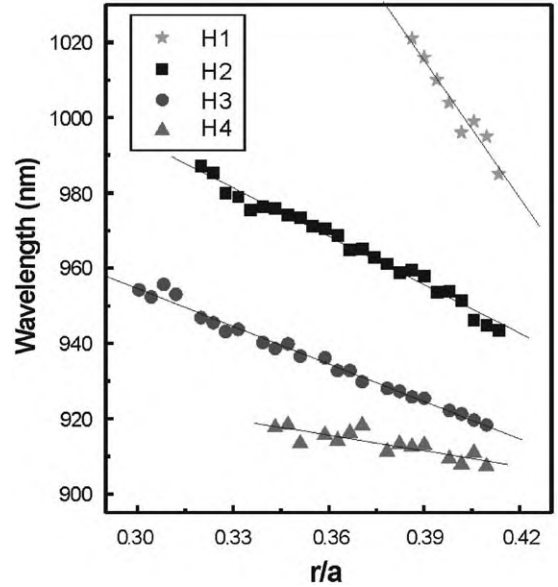


Fig. 2. Lower wavelength peak positions of the PCD modes as function of  $r/a$ , where  $r$  is the radius of the PC holes and  $a$  is the periodicity.

the slope of the data shown in Fig. 2a corresponds to a shift rate of  $d\lambda/d(r/a) \sim 1220$  nm. For  $a = 300$  nm, a 1% change of ( $r/a$ ) results in an absolute change of the effective cavity length of  $\sim 6$  nm. If we estimate for the effective length of a H1 cavity to be  $\sim 500$  nm (with  $r/a = 0.4$ ), this results in an effective length change of 1.2%. Thus, the calculated shift rate for a mode at  $\lambda = 1030$  nm is  $d\lambda/d(r/a) \sim 1240$  nm, in excellent accord with our experimental observations. Similar calculations were performed for all presented PCD modes, the results being summarized in Table 1.

For H1 and H3 cavities, excellent agreement is found between experiment and calculations indicating a direct dependence of the mode energy on the effective *lateral* size of the cavity. This observation indicates that electromagnetic field distribution of these modes should be orientated predominantly parallel to the waveguide, therefore a decrease of the air-fill factor would directly lead to an extension of the electromagnetic field distribution. In contrast, much poorer agreement is obtained for the most prominent H4 mode,

Table 1

Measured and calculated mode shift rates  $d\lambda/d(r/a)$  for the four cavity modes form Fig 1. In addition, the estimated effective length of the four investigated PCD cavity sizes is given

	H1 (nm)	H2 (nm)	H3 (nm)	H4 (nm)
Measured $d\lambda/d(r/a)$	1220	520	330	160
Calculated $d\lambda/d(r/a)$	1240	460	330	240
Eff. length	500	1100	1700	2300

suggesting that it may be orientated perpendicular to slab waveguide

The evidence presented for localized cavity PC defect cavity states together with a clear enhancement of the collected emission intensity for QDs on-resonance with the PCD-cavity modes when compared with QDs off resonance (see PL-spectra in Fig. 1) suggests the presence of cavity QED phenomena. The photon lifetime in our cavities is  $\sim 1$  ps, much shorter than the QD spontaneous emission lifetime ( $\tau_{\text{spont}}$ ). This indicates that light matter interaction remains in the weak coupling regime and can be described by a Purcell modification of the spontaneous emission lifetime by a factor  $F_p \propto Q/V_{\text{mode}}$ . From the results presented above, measured  $Q$ -factors increase only slightly with cavity size from H1 to H4. In contrast, the typical mode volume for a H4 cavity is  $\sim 20 \times$  larger than for H1 and the strongest cavity QED effects are, therefore, expected to occur for H1-cavities.<sup>1</sup>

The samples were excited with an equivalent CW power density of  $\sim 40 \text{ W/cm}^2$  to observe both s- and p-shell QD emission. Mono-exponential time transients were observed from which we extracted the  $\tau_{\text{spont}}$ . Results of these measurements as a function of detection energy are shown in Fig. 3, detecting either away from (●) or on (▽) the cavity. Also shown for comparison is the on-cavity measured PL spectrum.

The measurements performed off cavity clearly reveal a systematic, smooth reduction of  $\tau_{\text{spont}}$  to shorter emission wavelengths. This effect is well studied [10], arising from the reduction of the QD

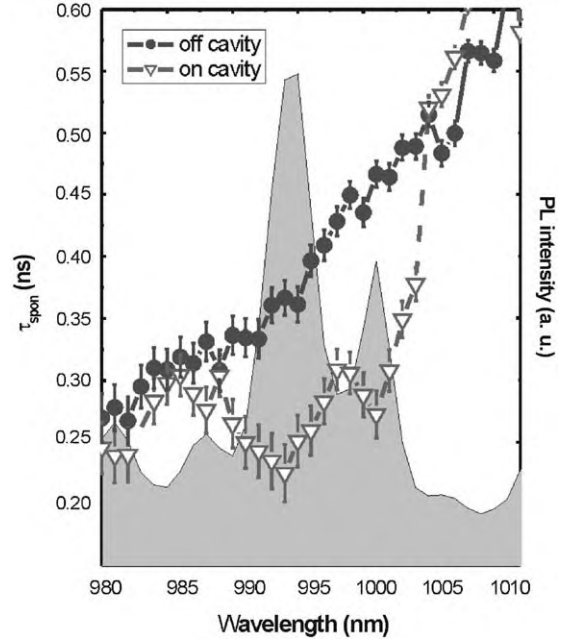


Fig. 3. Wavelength dependence of the excitonic decay lifetime in- and outside a H1 PCD. Grey shaded line gives the PL recorded from the cavity.

size and the modification of the exciton coherence volume in smaller QDs. In strong contrast, the data recorded on-cavity reveal two clear minima at the cavity modes whilst being similar to the off cavity data away from these modes. This observation clearly demonstrates a Purcell enhancement of  $\tau_{\text{spont}}$  on resonance, up to a factor  $\sim 2$  shortening having been observed. We note that the measurements of Fig. 3 were performed on a QD ensemble for which some dots may be energetically on resonance with the cavity mode whilst being spatially at a node of the optical field. Thus, the maximum Purcell enhancement in our structure may be significantly larger than that measured here. Single dot measurements are currently underway to clarify this expectation.

In summary, we have presented studies of QD based cavity QED phenomena. A clear Purcell enhancement of the light-matter interaction was observed for QDs on-resonance with cavity modes, Purcell factors of at least a factor  $\sim 2$  having been demonstrated.

<sup>1</sup>for a H1 mode with  $Q \sim 300$  and  $V \sim 20 (\lambda/2n)^3$  the calculated Purcell factor is  $F_p \sim 9$ .

## Acknowledgements

This work is supported financially by the DFG via SFB 631 “Festkörperbasierte Quanteninformationsverarbeitung: Physikalische Konzepte und Materialaspekte”—Project B3.

## References

- [1] N. Gisin, et al., Rev. Mod. Phys. 74 (2002) 145.
- [2] P. Michler, et al., Nature 406 (2000) 968.
- [3] O. Benson, et al., Phys. Rev. Lett. 84 (2000) 2513.
- [4] J. Hours, et al., Appl. Phys. Lett. 82 (2003) 2206.
- [5] E.M. Purcell, Phys. Rev. 69 (1946) 681.
- [6] K. Srinivasan, et al., Appl. Phys. Lett. 83 (2003) 1915.
- [7] J. Vučković, et al., Appl. Phys. Lett. 82 (2003) 2374.
- [8] T.F. Krauss, R.M. De La Rue, PIQE. 23 (1999) 51.
- [9] T.D. Happ, et al., Phys. Rev. B 74 (2002) 041303(R).
- [10] R. Heitz, et. al., Phys. Rev. B 56 (1997) 10435.
- [11] T. Yoshie, et al., Appl. Phys. Lett. 79 (2001) 114.
- [12] K. Hennessy, et al., Appl. Phys. Lett. 83 (2003) 3650.